

CONFERENCES AND SYMPOSIA PACS numbers: 01.10.Fv, **61.72. – y**, **62.20. – x**, **62.30. + d**, **75.47. – m**, **75.75. – c**, **85.75. – d**

Spintronics and nanomagnetism
(Scientific session of the Physical Sciences Division of the Russian Academy of Sciences, 25 April 2012)

DOI: 10.3367/UFNe.0182.201212g.1345

A scientific session of the Physical Sciences Division of the Russian Academy of Sciences (RAS), entitled "Spintronics and nanomagnetism", was held on 25 April 2012 at the conference hall of the Lebedev Physical Institute, RAS.

The agenda of the session announced on the RAS Physical Sciences Division website www.gpad.ac.ru included the following reports:

(1) **Zvezdin A K, Zvezdin K A** (Prokhorov General Physics Institute, Russian Academy of Sciences, Moscow), **Popkov A F** (National Research University 'Moscow State Institute of Electronic Technology', Moscow) "Spin moment transfer effects and their applications in spintronics";

(2) **Fraerman A A** (Institute for Physics of Microstructures, Russian Academy of Sciences, Nizhny Novgorod) "Magnetic states and transport properties of ferromagnetic nanostructures";

(3) **Panin V E, Egorushkin V E, Panin A V** (Institute of Strength Physics and Materials Science, Siberian Branch of the Russian Academy of Sciences, Tomsk) "Nonlinear wave processes in a deformable solid as in a multiscale hierarchically organized system".

Papers based on oral reports 2 and 3 are presented below.

PACS numbers: **75.47. – m**, **75.75. – c**, **85.75. – d**
DOI: 10.3367/UFNe.0182.201212h.1345

Magnetic states and transport properties of ferromagnetic nanostructures

A A Fraerman

1. Introduction

There are at least two motivating factors for research interests in the transport properties of ferromagnetic nanostructures. First, conducting ferromagnets, which are the ones to be discussed below, have their current carriers spin-polarized. Their energy spectra are split into two subbands, in one of which the occupying electrons align their spin projections parallel and, in the other, antiparallel to the magnetic moment of the sample. The spin 'splitting' compares to the Curie temperature of these materials to an order of magnitude. It may be considered that in ferromagnets there is a colossal 'exchange' field of strength $H \sim k_B T_c/\mu_B \sim 10^6 - 10^7$ Oe (k_B is the Boltzmann constant, and μ_B is the Bohr magneton). Prior to the discovery of giant magnetoresistance [1–2] (see also Ref. [3] on the tunneling version of the effect), such an 'exchange' field had not manifested itself in the transport and optical properties of ferromagnets, which were determined by the relatively weak spin-orbit interaction [4] rather than the Coulomb interaction. This discovery has greatly stimulated renewed efforts to study spin-dependent transport effects.

Second, nanostructure formation methods, which have been the subject of intense development in recent years, are an effective tool for controling the magnetic state of a ferromagnet. It is known [5] that the magnetization distribution in a ferromagnetic sample is determined by competition among the magnetic anisotropy, the exchange interaction, and the magnetostatic interaction. The magnetic domain structure that results from this competition is not universal, but rather depends on the sample shape and dimensions. Nanostructure patterning allows one to control these parameters and, hence, magnetization distribution in the most important nanometer range. As far as this range is concerned, the important special feature of ferromagnets is the presence in them of two characteristic scales: the domain wall thickness and the exchange length, both measuring tens of nanometers for transition metal ferromagnets.

Thus, the search for new transport and optical effects of an 'exchange' nature in ferromagnetic nanostructures constitutes a topical and exciting task. This report briefly reviews the relevant research that has been done at the Institute for Physics of Microstructures, RAS.

2. 'Exchange' versions of the Hall and diode effects

Let us start by examining phenomenologically the possibility of transport effects of an exchange nature in inhomogeneous ferromagnets.

In a conducting medium under the influence of a constant electric field **E**, an electric current density **j** arises in the following form

$$j_i = \sigma_{ik} E_k + \gamma_{ijk} E_j E_k + \ldots \quad (1)$$

where the linear and quadratic conductivity tensors depend on the sample's magnetic moment and its spatial derivatives.

A A Fraerman Institute for Physics of Microstructures, Russian Academy of Sciences, Nizhny Novgorod, Russian Federation
E-mail: andr@ipm.sci-nnov.ru

Uspekhi Fizicheskikh Nauk **182** (12) 1345 – 1357 (2012)
DOI: 10.3367/UFNr.0182.201212g.1345
Translated by E G Strel'chenko, S N Gorin; edited by A Radzig

Uspekhi Fizicheskikh Nauk **182** (12) 1345 – 1351 (2012)
DOI: 10.3367/UFNr.0182.201212h.1345
Translated by E G Strel'chenko; edited by A Radzig

The problem that faces us consists in determining these dependences. Restricting the discussion to nondissipative processes in media with a center of inversion, we conclude that the linear and nonlinear conductivity tensors contain terms of odd powers in the magnetic moment $\mathbf{M}$, with the σ_{ik} and γ_{ijk} tensors having terms with even and odd powers of spatial derivatives, respectively. Assuming the exchange interaction to be responsible for the effects we are looking for, let us require that the expression for the current (1) be invariant under the coherent rotation of the sample's magnetic moment [5, 6]. This means that conductivity tensors must not comprise convolutions of 'spatial' indices with 'magnetic' ones). With all of the above requirements met, the following equation is derived for the electric current flowing in an inhomogeneously magnetized conducting ferromagnet [7, 8]:

$$j_i = \sigma\left(\mathbf{M}\left[\frac{\partial \mathbf{M}}{\partial x_i}\times\frac{\partial \mathbf{M}}{\partial x_k}\right]\right)E_k + \gamma\left(\mathbf{M}\left[\frac{\partial \mathbf{M}}{\partial x_i}\times\frac{\partial^2 \mathbf{M}}{\partial x_j\,\partial x_k}\right]\right)E_jE_k + \ldots, \tag{2}$$

where σ, γ are the scalar constants (we confine ourselves to studying media with isotropic or cubic crystalline structures). The linear conductivity tensor, which is antisymmetric, describes the contribution of an exchange nature to the Hall effect, whereas the second term on the right-hand side of equation (2) is responsible for the rectifying properties of the ferromagnet. Both tensors found are nonzero only in those ferromagnets where the magnetic moment vectors do not lie in the same plane, i.e., in samples with noncoplanar magnetization distribution. To see that this is indeed the case, note that expressions for the conductivity tensors can be readily obtained by expanding the mixed product $\mathbf{M}_1[\mathbf{M}_2\times\mathbf{M}_3]$ in a Taylor series, where $\mathbf{M}_{1,2,3}$ are the magnetic moments at the neighboring points in the sample. If the linear conductivity tensor is different from zero in systems with a nononedimensional distribution of the magnetic moment, it follows that a sample with a one-dimensional noncoplanar magnetization distribution should also have rectifying properties.

Two examples of noncoplanar magnetic moment distribution are worth considering. Suppose a ferromagnet has a magnetization distribution of the form

$$\mathbf{M} = \big(\sin\theta(\rho)\,\cos(v\varphi+\varphi_0),\ \sin\theta(\rho)\sin(v\varphi+\varphi_0),\ \cos\theta(\rho)\big), \tag{3}$$

where φ, ρ are cylindrical coordinates, v is an integer, and φ_0 is a (constant) phase shift. Substituting Eqn (3) into expression (2) yields

$$\mathbf{j} = \mathbf{E}\times\mathbf{B}_{\text{eff}}, \qquad B_{\text{eff}} = \sigma\left(\mathbf{M}\left[\frac{\partial \mathbf{M}}{\partial x}\times\frac{\partial \mathbf{M}}{\partial y}\right]\right) = \sigma v\,\frac{1}{\rho}\,\frac{\partial\cos\theta}{\partial\rho}, \tag{4}$$

implying that a vortex ($v=1$, $\varphi_0=\pm\pi/2$) or an antivortex ($v=-1$, $\varphi_0=0,\pi$) noncoplanar magnetic moment distribution can be expected to provide an additional contribution to the Hall effect. For a distribution in the form of a conical magnetic spiral, namely

$$\mathbf{M}(z) = \big(m\cos(qz),\ m\sin(qz),\ m_z\big), \qquad \mathbf{M}^2 = m^2 + m_z^2, \tag{5}$$

the result of such a substitution reduces to

$$j_z = \gamma q^3 m_z(1-m_z^2)\,E_z^2, \tag{6}$$

suggesting the existence of diode properties in such a structure. A classical model proposed in Ref. [9] deduces the 'exchange' contribution to the Hall conductivity from the noncollinearity between the magnetic moment of a moving particle and the external field and can be used as a basis to explain, at least in part, the microscopic mechanism of the effects being discussed.

3. Optical and neutron-optical effects

To describe conduction electrons in ferromagnets, the simplest quantum-mechanical approach is to apply the Vonsovskii–Zener s-d model, in which the problem reduces to that of finding the eigenfunctions and eigenvalues of the Schrödinger equation

$$-\Delta\Psi(\mathbf{r}) - J\mathbf{M}(\mathbf{r})\,\hat{\boldsymbol{\sigma}}\,\Psi(\mathbf{r}) = E\Psi(\mathbf{r}), \tag{7}$$

where $\hat{\boldsymbol{\sigma}}$ is the Pauli matrix vector, J is the exchange interaction constant between the conduction s and localized d electrons, and $\mathbf{M}$ is the unit vector in the direction of the magnetic moment. Note the analogy between the s-d model description of conduction electrons in ferromagnets and the description of neutrons for which the magnetic moment vector in equation (7) should be replaced by the magnetic induction vector $\mathbf{B}$, and the exchange constant by the Bohr nuclear magneton [10]. This analogy provides a common framework for discussing the transport and optical properties of conducting ferromagnets, on the one hand, and neutron scattering by inhomogeneous magnetic systems, on the other hand.

For the case of a magnetic spiral defined by formula (5), equation (7) can be solved exactly [11] to yield the following expressions for the spectrum and eigenfunctions of the system:

$$E_\pm = k^2 + p^2 + \left(\frac{q}{2}\right)^2 \pm \sqrt{q^2k^2 + J^2 - 2m_zJqk}, \tag{8}$$

$$\Psi_\pm = \frac{1}{\sqrt{1+\delta_\pm(k)}}\begin{pmatrix}\delta_\pm(k)\exp\left(-\dfrac{\mathrm{i}qz}{2}\right)\\ \exp\left(\dfrac{\mathrm{i}qz}{2}\right)\end{pmatrix}\exp(\mathrm{i}kz)\exp(\mathrm{i}\mathbf{p}\boldsymbol{\rho}),$$

$$\delta_\pm = \frac{m_zJ - qk \pm \sqrt{q^2k^2 + J^2 - 2m_zJqk}}{J(1-m_z^2)^{1/2}}, \tag{9}$$

where k, $\mathbf{p}$ are the electron quasimomenta along and perpendicular to the spiral axis, respectively.

From expression (8) it follows that the spectrum of current carriers in a conical ($m_z\neq 0$) spiral is not an even function of quasimomentum. Thus, the electrons moving to the left along the spiral axis have different group velocities from those moving to the right. In a macroscopic system, this difference does not produce an electric current because it is exactly compensated for by the difference in the number of opposite-moving equilibrium electrons. In mesoscopic systems, however — such as small ferromagnetic rings with a noncoplanar distribution of the magnetic moment — the removal of Kramers degeneracy and the quantization of quasimomentum can lead to the appearance of predicted [12, 13] persistent electric currents.

In a conical magnetic spiral, spectral asymmetry is responsible for the occurrence of the diode effect, with 'easy' current flow direction being determined by the sign of the spiral wave number (left–right spiral) and by where the perpendicular magnetic moment component m_z is directed [see formula (6)]. The important point is that, as can be seen from Eqn (9), the wave function components — and hence the expectation value of the electron's intrinsic magnetic moment — depend on the quasimomentum component along the spiral axis. This results, in particular, in electron scattering by nonmagnetic impurities becoming asymmetric, thus adding to the diode effect [7]. Similar effects (asymmetry in both the group velocity and the scattering rate by nonmagnetic impurities) are responsible for the peculiarities in the spatial dispersion of the dielectric constant. For a conical magnetic spiral, the expansion of the dielectric constant may contain an additional term of the form [14]

$$\varepsilon_{ii} = K_{ii}\left(\mathbf{M}\left[\frac{\partial \mathbf{M}}{\partial z}\times\frac{\partial^2 \mathbf{M}}{\partial z^2}\right]\right)k_z\,, \tag{10}$$

where k_z is the spiral axis component of the electromagnetic wave vector.

Of special note is that the electric component of an electromagnetic wave can induce transitions between spin subbands in noncollinear and noncoplanar magnetic systems. Using the wave functions of Eqn (9), the probability of electric dipole transitions between spin subbands in a magnetic spiral is readily found to be [15]

$$W^{\pm}_{k,k'} = \frac{2\pi}{\hbar}\left(\frac{JeE_z q}{2m\omega^2}\right)^2 (1-m_z^2)\,\delta(\mathbf{k}-\mathbf{k}')\,\delta\big(\Delta E\,(k_z)-\hbar\omega\big), \tag{11}$$

where ω is the electromagnetic wave frequency, ΔE is the energy spacing between the spin subbands, and $\delta(x)$ is the delta function. In noncollinear systems, these transitions make an additional contribution to radiation absorption, as analyzed in detail in paper [16]. In a noncoplanar magnetic system (such as a conical magnetic spiral), the electric dipole transitions (11) give rise to a constant electric current, i.e., to the photogalvanic effect [15].

Let us consider some features of neutron scattering by noncoplanar magnetic systems. It is known [10] that the interaction between cold neutrons and a magnetic field is sufficiently weak for the scattering cross section to be representable as a power series in the magnetic induction **B**. The only factor determining the interaction between a magnetic field and a neutron spin is the angle between them. Hence, the total scattering cross section (summed over the spin polarizations of the incident and scattered neurons) should be invariant with respect to coherent rotation of the magnetic field at any point in space. Given the above, the scattering cross section can be expressed as

$$\begin{aligned}\sigma\big(\mathbf{k},\mathbf{k}',\mathbf{B}(\mathbf{r})\big) &= \sigma_0(\mathbf{k},\mathbf{k}')\\ &+\int Q_1(\mathbf{k},\mathbf{k}';\mathbf{r}_1,\mathbf{r}_2)\big(\mathbf{B}(\mathbf{r}_1)\,\mathbf{B}(\mathbf{r}_2)\big)\,\mathrm{d}\mathbf{r}_1\,\mathrm{d}\mathbf{r}_2\\ &+\int Q_2(\mathbf{k},\mathbf{k}';\mathbf{r}_1,\mathbf{r}_2,\mathbf{r}_3)\big(\mathbf{B}(\mathbf{r}_1)\big[\mathbf{B}(\mathbf{r}_2)\times\mathbf{B}(\mathbf{r}_3)\big]\big)\,\mathrm{d}\mathbf{r}_1\,\mathrm{d}\mathbf{r}_2\,\mathrm{d}\mathbf{r}_3+\ldots,\end{aligned} \tag{12}$$

where $\mathbf{k}$, $\mathbf{k}'$ are the incident and scattered neutron wave vectors, and $Q_{1,2}$ are the scalar functions. Because the scattering cross section should obey the reciprocity theorem $\sigma\big(\mathbf{k},\mathbf{k}',\{\mathbf{B}(\mathbf{r})\}\big)=\sigma\big(-\mathbf{k}',-\mathbf{k},\{-\mathbf{B}(\mathbf{r})\}\big)$, it follows that the last term in Eqn (12) describes the 'nonreciprocal' contribution, due to the noncoplanar nature of the magnetic induction distribution. Note that calculating this contribution requires going beyond the Born approximation commonly used in the calculation of the cold neutron scattering cross section. See Refs [17, 18] for a discussion of how the nonreciprocal features in the scattering of neutrons manifest themselves in noncoplanar magnetic structures.

Thus, based on the theoretical discussion above, a whole series of new and interesting effects — transport, optical and neutron-optical — are likely to occur in ferromagnetic nanostructures with a noncoplanar, specifically, vortex and spiral, magnetization distribution. Sections 4 and 5 describe methods for creating and experimentally investigating ferromagnetic nanostructures with chirally distributed magnetization.

4. Ferromagnetic nanostructures with vortex distribution of magnetization

The vortex distribution of magnetization [$\nu = 1$, $\varphi_0 = \pm\pi/2$ in formula (3)] is the ground state of a ferromagnetic disc, provided that the radius and height of the disc are larger than the exchange length $l_{\mathrm{ex}} \approx \sqrt{J/M_s^2} \sim 20$ nm [19]. The techniques we used to create such particles involved magnetron sputtering and electronic lithography (Supra 50 V microscope with a lithographical attachment ELPHY Plus) [8, 20, 21]. To effectively control the magnetic state of a nanostructured sample requires that both the geometric dimensions of the sample and its crystalline structure be controlled. For our purposes, polycrystalline samples with a crystallite size of ≈ 20 nm and a sufficiently low ($\approx 20-30$ Oe) coercive force are suitable. Magnetization curves of ferromagnetic films were measured magnetooptically before the lithography process began. The magnetic states of the particles were investigated by magnetic-force microscopy (Solver-HV vacuum probe microscope). The details of the probe measurements performed are presented in Refs [8, 20–22]. Using this method, the vortex state in elliptic ferromagnetic particles was studied in detail, as was the possibility of utilizing the magnetic tip of a probe microscope to control these states.

In symmetrically shaped particles, the magnetic vortex state is degenerate with respect to the vorticity direction, making the particles with left- and right-rotating vortices ($\varphi_0 = \pm\pi/2$) equal in number [23]. For asymmetrical (for example, triangular) particles (see Fig. 1a), if the magnetic field is applied along the triangle bases, it takes different field strengths to produce 'left' and 'right' vortices [24], thus allowing for a lattice of particles with the same sign of vorticity to be created. Shown in Fig. 1b is a magnetic-force image of the remanent state of a lattice of triangular particles. It is seen that all the particles have the same sign of vorticity which can be controlled by changing the direction of the demagnetizing magnetic field. What makes this system remarkable is the presence of a macroscopic toroidal magnetic moment $\mathbf{T} = (1/N)\sum_i [\mathbf{r}_i \times \mathbf{M}_i] \neq 0$, a fact which should, in turn, lead to nonreciprocality in light diffraction by such a lattice. Our recent experiments [25] completely confirmed this prediction.

It seems of interest to fabricate a nanostructure with the antivortex distribution of magnetic moment [$\nu = -1$, $\varphi_0 = 0, \pi$ in formula (3)]. For such a distribution, the Hall voltage reverses sign relative to that in the vortex system [see

formula (4)]. The integer v is a topological charge of the soliton [26, 27]. The direct proportionality between the Hall voltage and the topological charge of the magnetization distribution justifies naming this effect the 'topological' Hall effect [28]. That the antivortex state is difficult to realize is explained by the presence of excess (relative to the vortex state) magnetostatic energy proportional to the particle volume [8].

Our way to still achieve the goal was to make a lattice of cross-shaped ferromagnetic particles (Fig. 2a) with a feature of increased width on two of the four sides of the cross. The external magnetic field was applied at an angle of 45° to the sides of the cross-shaped particle, as shown by the arrow in Fig. 2a. The remanent states of the system following magnetization in external fields of 1 kOe and 250 Oe are shown in the respective Fig. 2b and 2c, corresponding, respectively, to the quasiuniform magnetic state of the crosses and to the antivortex state of the particles, the latter manifesting itself in that, close to the cross edges, the distribution of 'magnetic charges' changes its symmetry from dipole to quadrupole.

5. Ferromagnetic nanostructures with a spiral magnetization distribution

A noncollinear state can form in a multilayered ferromagnetic nanoparticle due to the magnetostatic interaction between the layers, the stability of the state being determined by the shape of the particle [29].

Let us consider three homogeneous magnetized magnetic discs with dielectric interlayers between them. The magnetostatic interaction between the layers is antiferromagnetic in character, resulting, as shown theoretically [30, 31], in the ground state of the system being spiral (provided that the interaction energy between the discs is much higher than the energy of anisotropy due to, for example, the disc shape). The magnetic state of a multilayered particle can be analyzed experimentally by examining the dependence of its electrical

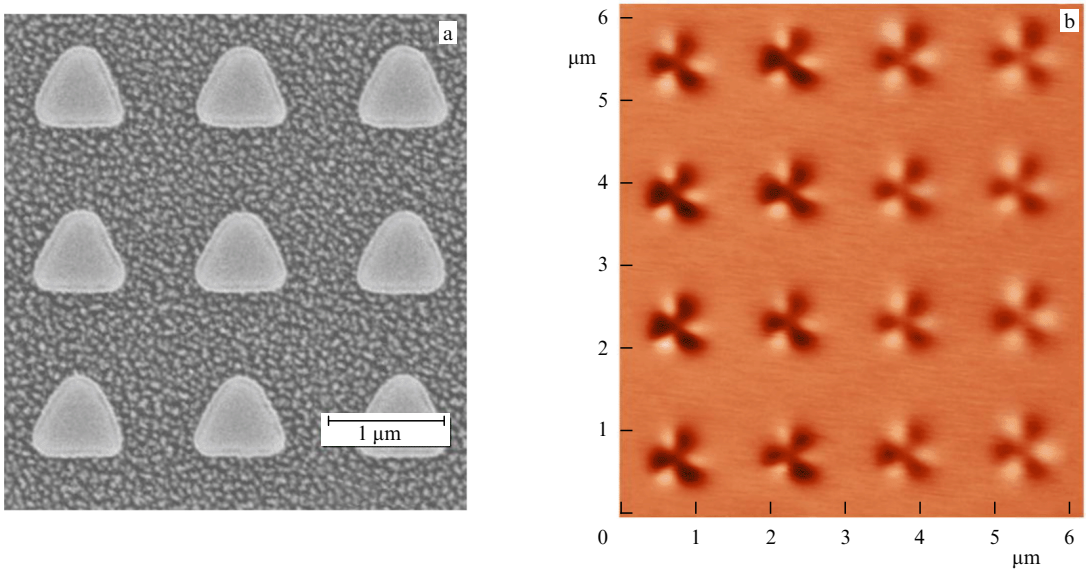

Figure 1. (a) Electron microscopic image of a lattice of triangular particles. (b) Magnetic-force image of the remanent state of this lattice following magnetization in a strong magnetic field applied along the triangle bases.

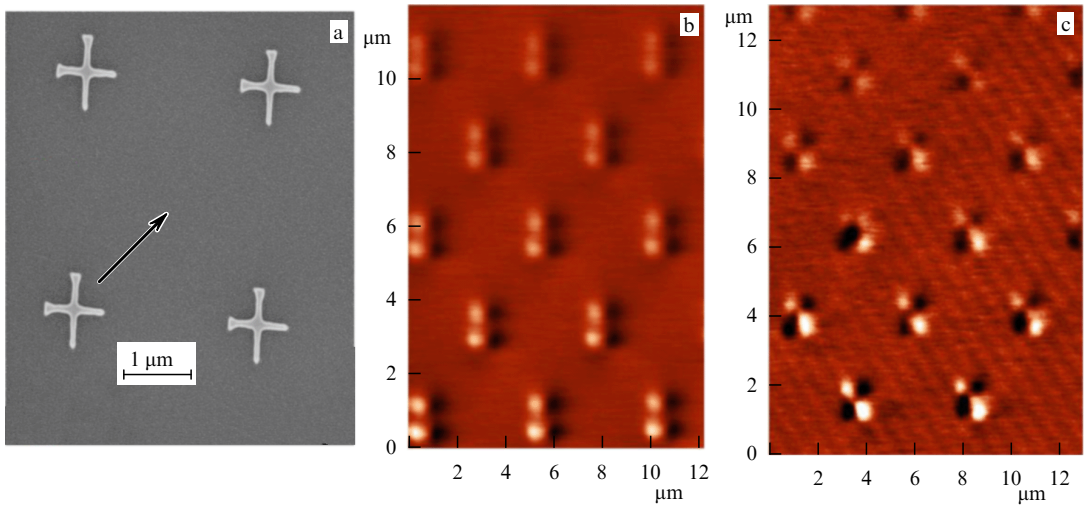

Figure 2. (a) Electron microscopic image of a lattice of cross-shaped particles. (b) Magnetic-force image of the remanent state of this lattice following magnetization in a 1-kOe external field applied in the direction shown by the arrow in Fig. 2a. (c) Magnetic-force image of the remanent state of the lattice of particles following the application of a 250-Oe field.

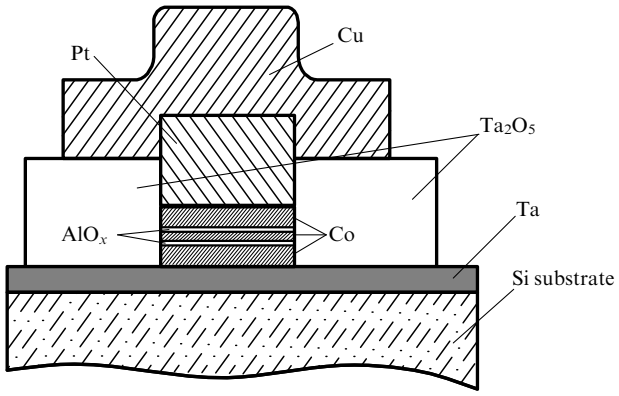

Figure 3. Schematic of a multilayered magnetic particle built into a thin-film electrode system.

resistance on the external magnetic field. Assuming that the field dependence is due to effects of an exchange nature and proportional to the scalar product of the layer magnetic moments [32], we have

$$R = R_{01} + R_{02} - R_1 \cos\theta_{12} - R_2 \cos\theta_{23}\,, \qquad (13)$$

where $\theta_{12}(\theta_{23})$ is the angle between the magnetic moments of the first and second (second and third) discs, R_{01}, R_1 (R_{02}, R_2) is the resistance of the first (second) tunnel junction for the disc magnetic moments oriented parallel, and $\theta_{12} = \theta_{23} = 0$. Alternatively, the magnetic states of multilayered particles can be investigated by magnetic-force microscopy, but the fact that the signal to measure is dominated by the contribution from the upper magnetic layer [30] makes this approach difficult to apply.

Figure 3 depicts a schematic of a multilayered magnetic particle built into a thin-film electrode system connected to a measuring device. The magnetic particle was prepared from a $Co(10\,nm)/AlO_x(2\,nm)/Co(5\,nm)/AlO_x(2\,nm)/Co(10\,nm)$ thin-film structure. We give elsewhere [29] a detailed description of the preparation method.

Figure 4a shows, for a circular particle ≈ 250 nm in diameter, the measured relative change in resistance, $r(H) = (R(H) - R(H \to \infty))/R(H \to \infty)$, as a function of the externally applied magnetic field (directed as shown by the arrow). The multilayered particle possesses a minimum resistance in large magnetic fields, $|H| > 400$ Oe, and a maximum resistance in low fields, $|H| < 200$ Oe. When the external magnetic fields are large, all the discs have their magnetic moments aligned and, according to formula (13), the resistance of the system is a minimum. As the magnetic field is decreased in magnitude, the layer magnetic moments dissalign, leading to increased resistance.

It is the region of small magnetic fields which is of particular interest. After reaching a maximum, the resistance of the system again decreases, and in a zero field its relative change is $r(0) \approx 0.75\, r_{\max}$, where $r_{\max}$ is the value of r at a maximum. Changing the direction of the external magnetic field results in a dramatic increase in the sample's resistance (segment A–B in Fig. 4a). As the field is increased further, the resistance reaches a maximum again. This resistance versus external magnetic field behavior suggests the layer magnetizations are distributed in a noncollinear fashion in a zero external field.

Suppose that the magnetic moment distribution corresponding to the resistance maximum is collinear 'antiferromagnetic', and that in the absence of a field the symmetric noncollinear state $\theta_{12} = \theta_{23} = \theta$ is realized. Then, using formula (13) and the experimental value $r(0) = 0.75\, r_{\max}$ yields $\theta \approx 120°$. Computer simulation results confirm this scenario.

As the particle anisotropy increases, the angular phases become unstable, resulting in the fact that the resistance versus magnetic field dependence has a number of features that correspond to transitions between collinear phases. The multilayered particles prepared had the same layer thickness as the first sample, but the layer lateral size was taken to be 100×200 nm. The ferromagnetic layers were taken to be CoFe films whose coercivity exceeded that of Co films but which allowed achieving the higher values of $r(H)$.

Figure 4b plots the relative change in the resistance of this sample as a function of the external field strength applied along the long axis of the particle. One does indeed see jumps in resistance which correspond to transitions between the

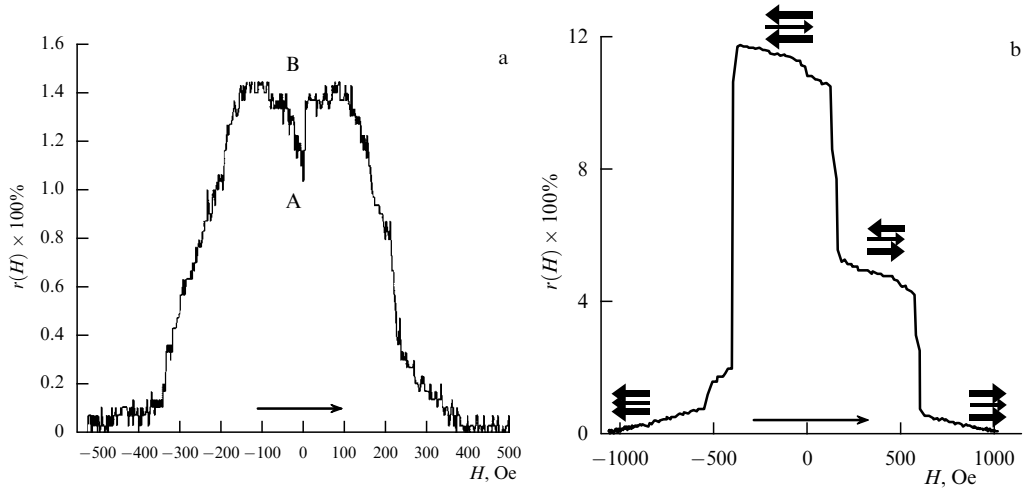

Figure 4. (a) Experimental $r(H)$ data for a circular particle 250 nm in diameter for layer thicknesses $Co(10\,nm)/AlO_x(2\,nm)/Co(5\,nm)/AlO_x(2\,nm)/Co(10\,nm)$; the arrow shows the direction of the change in the outer magnetic field. (b) The same for an 'elliptic' particle with lateral dimensions of 200×100 nm for layer thicknesses $CoFe(10\,nm)/AlO_x(2\,nm)/CoFe(5\,nm)/AlO_x(2\,nm)/\,CoFe(10\,nm)$; the magnetic field is directed along the long axis of the particle.

collinear states marked in the figure. Using experimental data, we find that the 'magnetically dependent' parts of transition resistances $R_{1,2}$ (see formula (13)) differ by 20% or less. There are two points to note from the results of this experiment. First, the two tunneling junctions in series that make up the structure under study share a sufficiently high degree of identity. Second, anisotropy plays a fundamental role in the formation of noncollinear states.

6. Conclusion

To summarize, this paper

— predicts new transport, optical, and neutron-optical effects for ferromagnetic systems with a noncoplanar magnetization distribution;

— develops nanolithography and probe microscopy techniques that create vortex, antivortex, and spiral magnetization distributions in ferromagnetic nanostructures;

— establishes that, in multilayered ferromagnetic particles of anisotropic shape, stable collinear states of different resistance exist, making these systems promising for application in information storage and processing devices.

While there has been some success in the study of inhomogeneously magnetized ferromagnetic structures, thus far none of the predicted 'exchange' effects have been observed. Noting also that many relevant topics are left unaddressed in this paper [including those related to the magnetoelectric effect in inhomogeneous magnets [33, 34], to phenomena in nonstationary and inhomogeneous magnetic structures (see, for example, Ref. [35]), etc.], it is safely concluded that the topic is far from exhausted and further research remains to be done.

Acknowledgments. This work was supported by RFBR (grants 11-02-00294-a, 11-02-00589-a, and 11-02-00434-a), by the programs 'Fundamental Studies in Nanotechnologies and Nanomaterials', 'Spin Phenomena in Solid-State Nanostructures and Spintronics', and 'Quantum Macrophysics' of the Russian Academy of Sciences, and by the Russian Federation Ministry of Education and Science.

References

1. Baibich M N et al. *Phys. Rev. Lett.* **61** 2472 (1988)
2. Binasch G et al. *Phys. Rev. B* **39** 4828 (1989)
3. Julliere M *Phys. Lett. A* **54** 225 (1975)
4. Vonsovskii S V *Magnetizm* (Magnetism) (Moscow: Nauka, 1971) [Translated into English (New York: J. Wiley, 1974)]
5. Landau L D, Lifshitz E M *Elektrodinamika Sploshnykh Sred* (Electrodynamics of Continuous Media) (Moscow: Nauka, 1982) [Translated into English (Oxford: Pergamon, 1984)]
6. Andreev A F, Marchenko V I *Usp. Fiz. Nauk* **130** 39 (1980) [*Sov. Phys. Usp.* **23** 21 (1980)]
7. Fraerman A A, Udalov O G *Phys. Rev. B* **77** 094401 (2008)
8. Mironov V L et al. *Phys. Rev. B* **81** 094436 (2010)
9. Aharonov Ya, Stern A *Phys. Rev. Lett.* **69** 3593 (1992)
10. Izyumov Yu A, Naish V E, Ozerov R P *Neitronografiya Magnetikov* (Neutron Diffraction of Magnetic Materials) (Moscow: Atomizdat, 1981) [Translated into English (New York: Consultants Bureau, 1991)]
11. Matveev V M, Nagaev É L *Zh. Eksp. Teor. Fiz.* **69** 2151 (1975) [*Sov. Phys. JETP* **42** 1094 (1975)]
12. Loss D, Goldbart P, Balatsky A V *Phys. Rev. Lett.* **65** 1655 (1990)
13. Tatara G, Kohno H *Phys. Rev. B* **67** 113316 (2003)
14. Karashtin E A, Udalov O G, Fraerman A A *Zh. Eksp. Teor. Fiz.* **136** 1127 (2009) [*JETP* **109** 973 (2009)]
15. Fraerman A A, Udalov O G Pis'ma *Zh. Eksp. Teor. Fiz.* **87** 187 (2008) [*JETP Lett.* **87** 159 (2008)]
16. Karashtin E A, Udalov O G *Zh. Eksp. Teor. Fiz.* **140** 1134 (2011) [*JETP* **113** 992 (2011)]
17. Ignatovich V K, Nikitenko Yu V, Fraerman A A *Zh. Eksp. Teor. Fiz.* **137** 886 (2010) [*JETP* **110** 775 (2010)]
18. Tatarskii D A, Udalov O G , Fraerman A A *Zh. Eksp. Teor. Fiz.* **142** 710 (2012) [*JETP* **115** 626 (2012)]; arXiv:1101.2735
19. Cowburn R P et al. *Phys. Rev. Lett.* **83** 1042 (1999)
20. Mironov V L et al. *J. Appl. Phys.* **106** 053911 (2009)
21. Chang J et al. *J. Appl. Phys.* **100** 104304 (2006)
22. Mironov V L et al. *Fiz. Met. Metalloved.* **110** 708 (2010) [*Phys. Met. Metallogr.* **110** 708 (2010)]
23. Vdovichev S N et al. *Fiz. Tverd. Tela* **48** 179 (2006) [*Phys. Solid State* **48** 1902 (2006)]
24. Yakata S et al. *Appl. Phys. Lett.* **97** 222503 (2010)
25. Udalov O G et al., arXiv:1204.2461
26. Kosevich A M, Ivanov B A, Kovalev A S *Nelineinye Volny Namagnichennosti*: *Dinamicheskie i Topologicheskie Solitony* (Nonlinear Magnetization Waves: Dynamical and Topological Solitons) (Kiev: Naukova Dumka, 1983)
27. Kosevich A M, Ivanov B A, Kovalev A S *Phys. Rep.* **194** 117 (1990)
28. Neubauer A et al. *Phys. Rev. Lett.* **102** 186602 (2009)
29. Vdovichev S N et al. *Pis'ma Zh. Eksp. Teor. Fiz.* **94** 418 (2011) [*JETP Lett.* **94** 386 (2011)]
30. Fraerman A A et al. *J. Appl. Phys.* **103** 073916 (2008)
31. Mukhamatchin K R, Fraerman A A *Pis'ma Zh. Eksp. Teor. Fiz.* **93** 797 (2011) [*JETP Lett.* **93** 716 (2011)]
32. Slonczewski J C *Phys. Rev. B* **39** 6995 (1989)
33. Zvezdin A K, Pyatakov A P *Usp. Fiz. Nauk* **179** 897 (2009) [*Phys. Usp.* **52** 845 (2009)]
34. Zvezdin A K, Pyatakov A P *Usp. Fiz. Nauk* **182** 593 (2012) [*Phys. Usp.* **55** 557 (2012)]
35. Fraerman A A, Muhamatchin K R, Tokman I D *Phys. Rev. B* **84** 012402 (2011)

PACS numbers: **61.72.–y**, **62.20.–x**, **62.30.+d**
DOI: 10.3367/UFNe.0182.201212i.1351

Nonlinear wave processes in a deformable solid as in a multiscale hierarchically organized system

V E Panin, V E Egorushkin, A V Panin

1. Introduction

In this report, we theoretically and experimentally substantiate the conception of a multiscale description of a deformable solid as a nonlinear hierarchically organized system. The surface layers and all internal interfaces are considered as an independent planar functional subsystem with a short-range order. The channelled plastic flow in the planar subsystem is primary. It is responsible for the formation and emission of all types of strain-induced defects into the crystalline subsystem. This process is developed through the mechanism of nonlinear waves which determine the law of self-consistency of

V E Panin, V E Egorushkin, A V Panin Institute of Strength Physics and Materials Science, Siberian Branch of the Russian Academy of Sciences, Tomsk, Russian Federation
E-mail: paninve@ispms.tsc.ru

Uspekhi Fizicheskikh Nauk **182** (12) 1351 – 1357 (2012)
DOI: 10.3367/UFNr.0182.201212i.1351
Translated by S N Gorin; edited by A Radzig

plastic flow in hierarchically organized systems. The fracture is related to a wave-like structural phase decomposition of the material.

The science of plasticity and strength of solids is going through a stage of replacing a paradigm. For a long time, the description of plastic deformation and fracture of solids was developed in terms of linear approximations of the mechanics of continuum media (macroscale level) and of the physics of strain-induced defects in a loaded solid (microscale level). However, it has become obvious in recent decades that a deformable solid represents a multiscale hierarchically organized system which should be described in terms of nonlinear mechanics and nonequilibrium thermodynamics [1].

At present, mechanisms of deformation on the nano-, micro-, meso-, and macroscale levels are being widely discussed in the literature. Unfortunately, the classification of scales reduces in most cases to only the size factor, retaining within the single-level approach. The problems of a multiscale self-organization and allowance for the nonlinearity of a hierarchically organized system have so far remained undeveloped.

A fundamentally new proposition in the multiscale approach is the conception of classification of surface layers and all internal interfaces as functional nonlinear planar subsystems in which translational invariance is absent [3–5], rather than as planar defects in crystals (according to the approach accepted, e.g., in monograph [2]).

The primary plastic shears emerge not in a translationally invariant crystal but rather in planar strongly excited subsystems in the form of nonlinear waves of channelled local structural transformations. Upon such wave fluxes propagating in a planar subsystem, strain-induced defects of various types are generated. A periodic emission of defects into the crystalline subsystem is developed as a nonlinear wave process. The thermodynamic stability of the crystalline subsystem in the course of plastic deformation decreases continuously, causing a nonlinearity of the behavior of the deformable solid.

This paper is devoted to a theoretical and experimental substantiation of the fundamental importance of the role of nonlinear waves in the plastic deformation and fracture of solids.

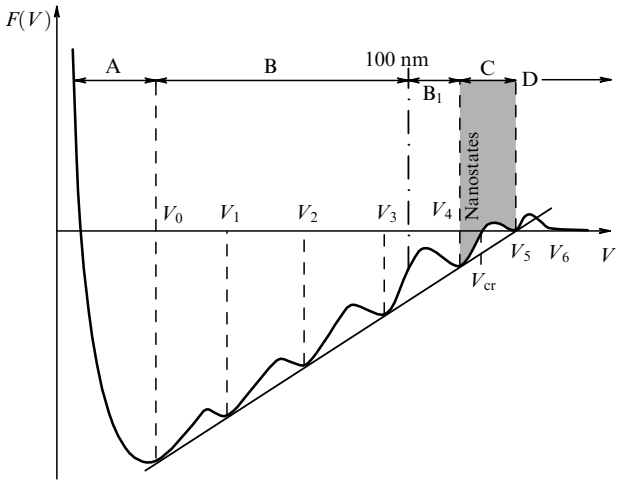

Figure 1. Dependence of the Gibbs thermodynamic potential $F(V)$ on the molar volume V with allowance for local zones of hydrostatic tension of various scales, in which defect structures arise. The regions of different states are as follows: A, hydrostatic compression; B, mesosubstructures of various structural scale levels; B_1, nano-sized structures, C, nanostructured states, and D, the emergence of porosity and fracture.

2. Nonlinear waves of channelled local structural transformations in a planar subsystem as the main mechanism of generating strain-induced defects. Law of plastic deformation flow self-consistency at various structural scale levels

Figure 1 illustrates the thermodynamic foundations of the evolution of the nucleation of strain-induced defects as local structural transformations by the example of the curve tracing the dependence of the Gibbs thermodynamic potential $F = F(V)$ on the molar volume V which is considered as a generalized thermodynamic parameter [3]. It follows from the expression $F = U - TS + PV - \sum_{i=1}^{n} \mu_i C_i$ that with increasing F in a deformable solid body, due to the presence of the terms U and PV, local minima can appear caused by the production of entropy and a redistribution of alloying elements (or impurities). In accordance with the nonequili-

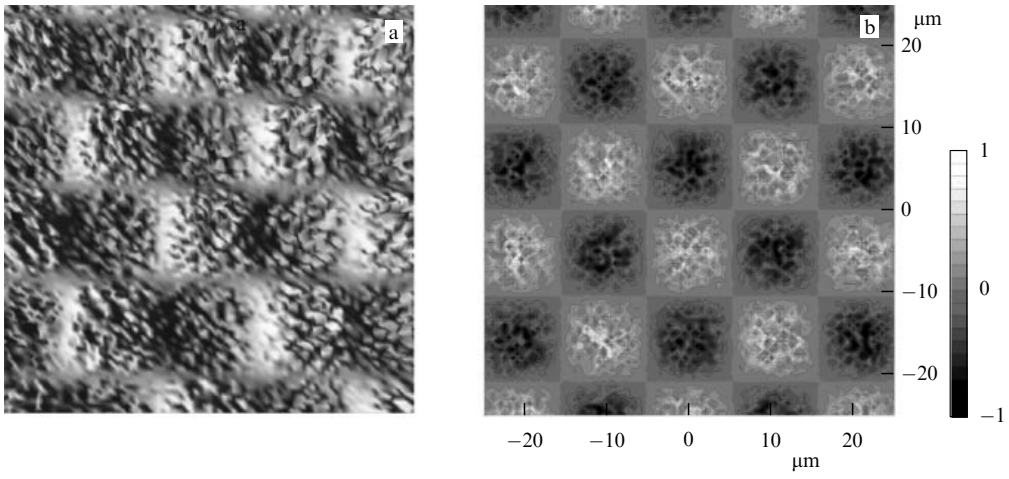

Figure 2. A 'chessboard' deformation profile on the surface of a deformable material; elasticity modulus of the surface layer is $E_s = 0.5E_b$ (where E_b is the appropriate elasticity modulus of the material's bulk). The thickness of the substrate was assumed to be infinitely large as compared to the thickness of the surface layer [7].

brium thermodynamics [6], zones of nonequilibrium states arise in a deformable crystal with increasing V because of the appearance in it of an inhomogeneous mechanical field. In these states, the entire set of strain-induced defects is formed, i.e., dislocations, disclinations, and mesobands and macrobands of localized plastic deformation. Finally, for $V > V_{cr}$, when the potential $F(V)$ becomes positive, the crystal in local zones of strongly nonequilibrium states loses thermodynamic stability and undergoes a structural phase decomposition. Cracks (or pores) are formed in such zones because of the excess molar volume.

The treatment of a deformable solid as a nonlinear multiscale system made it possible to establish the mechanisms of the formation of local zones of strongly nonequilibrium states, in which strain-induced defects of various scale levels are nucleated [3]. The necessity of self-consistency of shears at different structural-scale levels and the 'chessboard' character of the distribution of tensile and compressive normal stresses at the interfaces of structural subsystems (Fig. 2) [7] is responsible for the propagation of nonlinear waves of channelled local structural transformations in a solid under deformation. The appearance of zones of nonequilibrium states is associated with such nonlinear waves, with relaxation of these states occurring as a result of the generation of strain-induced defects in the crystalline subsystem. The effect of channeling fluxes of local structural transformations on mesoscale levels is a necessary condition for the propagation of multiscale nonlinear waves with allowance for the dissipative process of dislocation motion at the microscale level.

The multiscale development of nonlinear waves of plastic flow was predicted in our theoretical work [8–10]. The results of experimental investigations of such processes were generalized in Refs [3, 11–19].

In Refs [12–14, 18], the nonlinear waves of channelled plastic flow have been studied in the course of uniaxial tension in nanostructured surface layers of planar metallic samples and in thin films deposited onto a substrate. In all cases, nonlinear waves in the form of double spirals have been revealed (Figs 3, 4). Their quantitative treatment made it possible to compare the experimental data with the results of the scaling theory of nonlinear waves [10], which is described in Section 3.

3. Gauge theory of nonlinear waves of channelled local structural transformations

The introduction of dislocations and disclinations into the mechanics of a deformable solid is performed on the basis of the gauge theory of defects [20–22]. In papers [8–10], we suggested considering, as a group of gauge transformations, a simple nine-parameter group of transformations of a real three-dimensional space, GL(3, R); we also introduced sources of Yang–Mills fields — quasielastic microdistortions. The wave equations obtained, when analyzed with allowance for the nonequilibrium thermodynamics of discrete subsystems, make it possible to substantiate, in terms of the multiscale approach, both the wave nature of the channelled plastic deformation and the dissipative process of motion of strain-induced defects on a common structural scale level.

One of the particular cases of wave equations derived in paper [10] concerns the equations for the dimensionless quantities of the flux $\mathbf{J}$ and the density α of linear defects

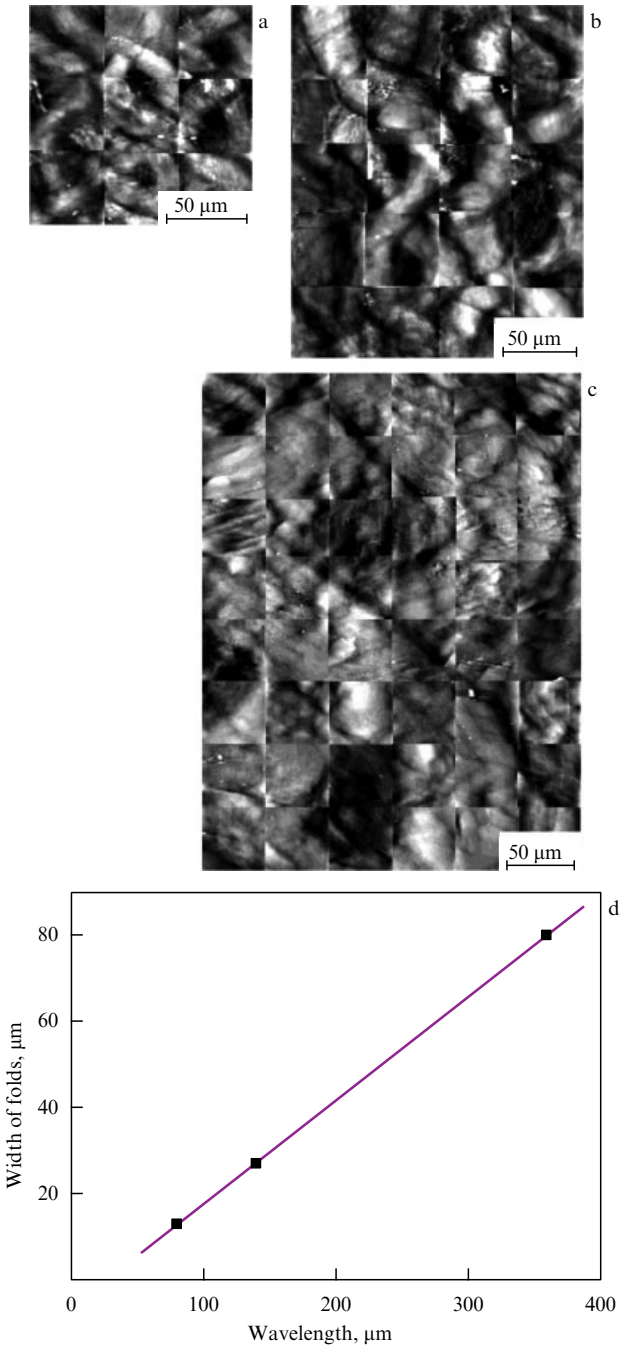

Figure 3. Double spirals of the extruded material in the mesobands of channelled deformation on the surface of planar samples of ferritic–martensitic steel with a nanostructured surface layer subjected to various tension ε: (a) $\varepsilon = 17\%$, the layer thickness is 100 μm; (b) $\varepsilon = 16\%$, the layer thickness is 200 μm, and (c) $\varepsilon = 10\%$, the layer thickness is 300 μm. The temperature reaches 293 K [14]. (d) Linear dependence of the width of the mesoband on the wavelength of double spirals.

(discontinuities of the displacement vector $\mathbf{u}$):

$$\frac{\partial}{\partial x_\alpha} J_\mu^\alpha = -\frac{\partial \ln u_\mu}{\partial t}\,, \tag{1}$$

$$\varepsilon_{\mu\chi\delta}\frac{\partial J_\delta^\alpha}{\partial x_\chi} = -\frac{\partial \alpha_\mu^\alpha}{\partial t}\,, \tag{2}$$

$$\frac{\partial \alpha_\mu^\alpha}{\partial x_\alpha} = 0\,, \tag{3}$$

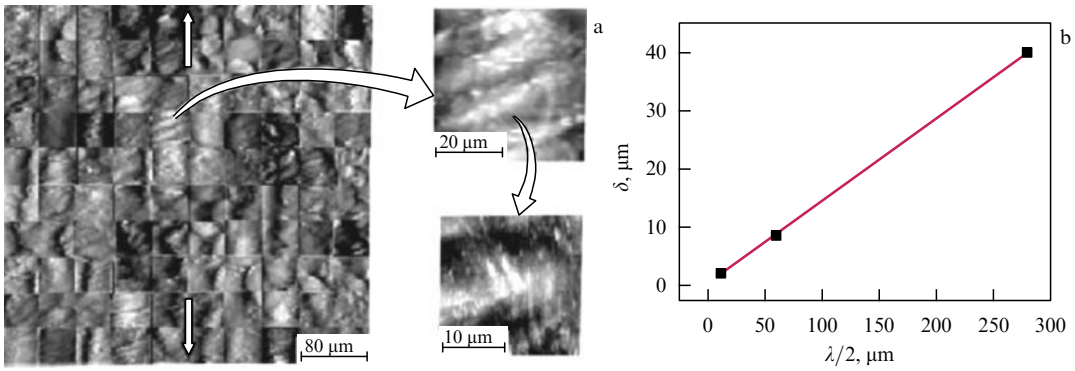

Figure 4. (a) Nonlinear waves in the form of double spirals on the surface of a sample of commercial titanium VT1-0 subjected to tension $\varepsilon = 16\%$ at $T = 293$ K after preliminary ultrasonic treatment and electrolytic hydrogenation for 1 h. The micrographs were obtained using scanning tunneling microscopy [18]. (b) Linear dependence of the thickness of extruded lamellae of various scales on their length.

$$\varepsilon_{\mu\chi\delta}\,\frac{\partial\alpha_\delta^\alpha}{\partial x_\chi} = \frac{1}{\tilde{c}^2}\,\frac{\partial J_\mu^\alpha}{\partial t} + \sigma_\mu^\alpha - P_\nu^\beta\,\frac{C_{\alpha\beta}^{\mu\nu}}{E}\,, \tag{4}$$

$$\frac{1}{c^2}\,\frac{\partial v_\mu}{\partial t} = \frac{\partial\sigma_\mu^\alpha}{\partial x_\alpha} - \frac{\partial P_\nu^\beta C_{\alpha\beta}^{\mu\nu}}{\partial x_\alpha E}\,, \tag{5}$$

where $v_\mu = \partial \ln u_\mu/\partial t$ is the rate of the elastic deformation of the medium with defects; $\sigma_\mu^\alpha = \partial \ln u_\nu/\partial x_\beta\ (C_{\alpha\beta}^{\mu\nu}/E)$ are the elastic stresses in such a medium; c and $\tilde{c}$ are the speed of sound and the speed of propagation of the plastic disturbance front, respectively; $P_\nu^\beta(x,t)$ is the plastic part of the distortion; $\varepsilon_{\mu\chi\delta}$ is the Levi–Civita symbol, and, finally, $C_{\alpha\beta}^{\mu\nu}$ are the elastic constants.

Equations (1)–(5) have the following meaning: (1) is the equation of the continuity of the medium with defects, from which it follows that the source of the plastic flow is the rate of the rearrangement of defects; (2) is the condition of the compatibility of plastic deformation [it is fundamentally important that the change in the density of the medium in time is determined in this case by the operation rot of the flux (i.e., by its spatial inhomogeneity), rather than by the operation div]; (3) is the condition of the continuity of defects, which reflects the absence of charges of the vortex component of a field of plastic deformation ($\alpha_\chi^\beta = \varepsilon_{\chi\mu\nu}\,\partial_\mu P_\nu^\beta$); (4) is the constitutive equation for a medium with plastic flow, and (5) is the equation of the quasielastic equilibrium, which in fact is an equation known in continuum mechanics, but here contains in its right-hand part, apart from the term responsible for elastic deformation, a term that describes plastic distortions, which in fact reflects the generation of strain-induced defects in local zones of hydrostatic extension produced by the stress concentrator.

Equation (4), which is inherent only in a medium with plastic flow, relates the temporary changes in the plastic flux to the anisotropic spatial changes in the densities of defects ($\varepsilon_{\mu\chi\delta}\,\partial\alpha_\delta^\alpha/\partial x_\chi$) and sources ($\sigma_\mu^\alpha - P_\nu^\beta C_{\alpha\beta}^{\mu\nu}/E$). The difference of equations (4) and (5) and the corresponding equations of the theory of elasticity lies in the fact that the change in the rate of plastic deformation with time is determined by the stresses themselves rather than by the derivatives $\partial\sigma_\mu^\alpha/\partial x$, as in the elastic case. In addition, the right-hand part of equation (4) contains, as a source, the plastic distortion $P_\nu^\beta(x,t)$ itself, which indicates the dual nature of the defects as field sources.

From the set of equations (1)–(5), we can derive wave equations for the dimensionless quantities of the flux density **J** and the defect density α:

$$\frac{1}{\tilde{c}^2}\,\frac{\partial^2 J_\alpha^\mu}{\partial t^2} - \frac{\partial^2 J_\alpha^\mu}{\partial x_\nu^2} = \frac{\partial}{\partial t}\left(\frac{\partial \ln u_\alpha(x,t)}{\partial x_\mu} - \frac{1}{E}\,\frac{\partial \ln u_\beta}{\partial x_\nu}\,C_{\alpha\beta}^{\mu\nu} - \frac{1}{E}\,P_\nu^\beta C_{\alpha\beta}^{\mu\nu}\right), \tag{6}$$

$$\frac{1}{\tilde{c}^2}\,\frac{\partial^2 \alpha_\alpha^\mu}{\partial t^2} - \frac{\partial^2 \alpha_\alpha^\mu}{\partial x_\nu^2} = \varepsilon_{\mu\chi\sigma}\left(\frac{\partial^2 \ln u_\beta(x,t)}{\partial x_\chi \partial x_\nu}\,C_{\alpha\beta}^{\sigma\nu} - \frac{\partial P_\nu^\beta}{\partial x_\chi}\,C_{\alpha\beta}^{\sigma\nu}\right)\frac{1}{E}\,, \tag{7}$$

under the condition of the compatibility of the sources:

$$\frac{\partial N_\mu}{\partial t} + \varepsilon_{\mu lm}\,\frac{\partial M_m}{\partial x_l} = 0\,, \tag{8}$$

where M stands for the right-hand side of Eqn (6), N is the right-hand side of Eqn (7), and $u(x,t)$ are the inelastic displacements in the inelastic localized strain wave.

The right-hand side of equation (6) characterizes the sources of the defect flux, which are determined by the rate of the quasielastic deformation, $\partial/\partial t\,(E_\mu^\alpha E - E_\nu^\beta C_{\alpha\beta}^{\mu\nu})\,(1/E)$, where E_μ^α and E_ν^β are the spherical and deviator components of the strain tensor, respectively, and $E_\mu^\alpha E - E_\nu^\beta C_{\alpha\beta}^{\mu\nu}$ is the difference in the internal stresses of compression–tension and shear, which are related to the distribution of stresses in the zone of the stress concentrator. The relaxation processes of the defect rearrangement (of the type of clusters of various atomic configurations or their conglomerates) are represented in equation (6) by the term $P_\nu^\beta C_{\alpha\beta}^{\mu\nu}/E$.

The right-hand side of equation (7) characterizes the source of the strain-induced defect density, which is represented by the vorticity $\varepsilon_{\mu\chi\delta}\,\partial/\partial x\,(E_\nu^\beta - P_\nu^\beta)\,(C_{\alpha\beta}^{\mu\nu}/E)$ of the shear deformation caused by the relaxation of shear stresses upon the generation of strain-induced defects in local zones of hydrostatic tension.

The character of the wave fluxes of strain-induced defects is determined by the right-hand side of equations (6) and (7). The plastic distortion $P_\nu^\beta(x,t)$ plays a fundamentally important role here.

Prior to the interpretation of equations (1)–(7), note that the wave equations of the plastic flow in solids have also been

obtained in papers [20–22], but they have not been interpreted there as plastic waves. The conclusion on the wave character of the propagation of a disturbance in a medium is always connected with the problem of the disturbance group velocity. In the absence of a dispersion of the group velocity, a wave is well defined. The inhomogeneity of a single-scale medium leads to a dispersion and the splitting of a wave packet. Therefore, in terms of the single-scale approach, no plastic waves can arise at all.

However, the conclusion on the existence of nonlinear plastic and fracture waves obtains convincing substantiation when a deformable solid is considered as a multiscale system, with allowance for the presence of planar subsystems in the form of surface layers and internal interfaces. Moreover, it is impossible to ensure beyond the scheme of nonlinear waves the reproduction of stress concentrators upon the propagation of plastic shears as local structural transformations.

Let us consider a localized flux of defects in a planar structure where the deformation along the direction L is developed as channeling between two layers of a crystalline material. Let us choose the common coordinate system so that the z-axis is oriented along L, while the x and y coordinates are varied within the thickness of the deformable layer. According to paper [10], the distribution of the plastic flux in the local ($r < L$) region has the form

$$\mathbf{J} = \frac{b_1 - b_2}{4\pi}\,\chi(s,t)\,\mathbf{b}(s,\mathbf{t}_\mathrm{n})\left(\ln\frac{2L}{r} - 1\right) - \nabla f, \tag{9}$$

where $\mathbf{b}$ is the vector of the binormal in the local coordinate system (perpendicular to the normal to a turn of the wave spiral and to its tangent); χ is the change in the curvature of the region (the change in the curvature of the axis of the region) caused by the external load; $\mathbf{t}_\mathrm{n}$ is the tangent; s is the current value of the region length; b_1, b_2 are the moduli of the so-called Burgers vector of the bulk translational and subsurface or rotational incompatibility, respectively, and ∇f is the gradient part of the flux caused by foreign sources.

Let us determine the change in the shape of the region of the localized deformation flux of length L with the initial dimensions δ. The space–time changes in the shape of $\mathbf{E}(s,t)$ in the process of deformation can be found from the equation

$$\mathbf{J} = \frac{\partial\mathbf{E}(s,t)}{\partial t}\,. \tag{10}$$

Using the expressions for $\mathbf{J}$ and making a replacement $t' \to t(b_1 - b_2)/(4\pi)[\ln(2L/r) - 1]$, we arrive at

$$\frac{\partial\mathbf{E}(s,t)}{\partial t} = \chi\mathbf{b} - \frac{4\pi}{(b_1 - b_2)[\ln(2L/r) - 1]}\,\nabla f. \tag{11}$$

The first term on the right-hand side of equation (11) describes the curvature of the defect flux (its vorticity). By solving equation (11) simultaneously with the equation $\partial\mathbf{E}/\partial s = \mathbf{t}$ and with Frenet equations [23], it can be shown that the change in the shape of the region under consideration is described as follows:

$$E_x(s,t) = -\frac{2}{\beta(v^2+1)}\left\{\operatorname{sech}\left[2\beta(s+4vt)\right]\sin\left[2\beta(s+4vt)\right] - \operatorname{sech}(8\beta vt)\,\sin(8\beta vvt)\right\}, \tag{12}$$

$$E_y(s,t) = -\frac{2}{\beta(v^2+1)}\left\{\operatorname{sech}\left[2\beta(s+4vt)\right]\cos\left[2\beta(s+4vt)\right] - \operatorname{sech}(8\beta vt)\,\cos(8\beta vvt)\right\}, \tag{13}$$

$$E_z(s,t) = s - \frac{1}{\beta(v^2+1)}\left\{\tanh\left[2\beta(s+4vt)\right] - \tanh(8\beta vt)\right\}. \tag{14}$$

Equations (12)–(14) govern the change in the shape of the region whose axis is a spiral curve with a constant torsion $\tau = 2v$. In these equations, $v = -v/\beta$, where v characterizes the velocity of the displacement of local structural transformations in the region of the spiral curve along the direction L, and the parameter β is related to the curvature χ as follows:

$$\chi(s,t) = 4\beta\operatorname{sech}\left[2\beta(s+4vt)\right]. \tag{15}$$

The curvature χ of the spiral is an important parameter of the channelled wave propagation of the localized plastic flow. The influence of this parameter on the shape of the spiral and on the local velocity v of the transverse change in the shape of the deformable region is illustrated in Fig. 5. As is seen from Fig. 5a, the velocity v of the transverse change in the shape is small at a slight curvature χ, and the spiral suffers a weakly pronounced torsion with a large transverse wavelength. Such a picture is observed when the plastic shear is developed under strongly nonequilibrium conditions, e.g., in nanostructured surface layers. With increasing curvature χ, the transverse wavelength decreases sharply, and the rates of the transverse shape changes increase (Fig. 5b). This is a very important effect, since in the zones of strong curvature a sharp increase is observed in the local effective potential $U(V,\alpha)$ in the expressions for the nonequilibrium Gibbs thermodynamic potential $F(V,\alpha) = F(V) - U(V,\alpha)$, where α characterizes the field of disturbances caused by the local violation of the translational invariance of the crystal [6]. This leads to a decrease in $|F(V,\alpha)|$, an increase in the molar volume V in the zone of curvature, and an increase in the rates of all types of atomic redistributions. After the condition $V > V_\mathrm{cr}$ is

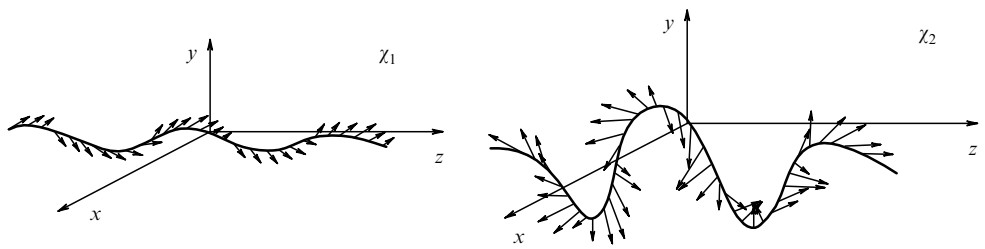

Figure 5. Dependences of the shape and rate of localized plastic deformation on the curvature χ of the region under deformation; $\chi_1 < \chi_2$.

reached, a structural–phase decomposition of the crystalline state occurs in the zone of strong curvature, and the material undergoes fracture. The manifestation of this effect is widely known in engineering practice.

4. Experimental verification of predictions of the gauge theory of nonlinear waves of channelled plastic deformation

Figure 3 displays nonlinear plastic waves that were channelled in nanostructured surface layers of planar samples of a ferritic–martensitic steel under conditions of uniaxial tension [14]. The observation of these waves makes it possible to perform an experimental verification of the predictions of the gauge theory of wave deformation in planar subsystems. A change in the thickness of the nanostructured surface layer leads to a change in both the nonlinear wavelength λ and the width δ of the spiral channelled flux. From formula (9), an expression that relates δ to λ can easily be obtained. According to paper [10], one has

$$\delta = L \exp\left[-\frac{4\pi(\nabla f \mathbf{b})}{\chi(b_1 - b_2)} \right]. \qquad (16)$$

At a given counter field ∇f from the side of the crystalline substrate, we obtain a scalar product $\nabla f \mathbf{b} = 0$ if $\nabla f \perp \mathbf{b}$. This condition corresponds to the double spirals of the extruded material shown in Fig. 3. This statement is especially well illustrated by the structure of nonlinear waves in titanium samples with a surface layer enriched in hydrogen [18]. The mechanism of extrusion of the surface layer material in a nonlinear wave has been investigated in Ref. [18] in the course of a uniaxial tension of planar samples of polycrystalline titanium whose surface layers were nanostructured and enriched in hydrogen. Titanium has a very low shear stability (a stacking-fault energy of only 10 mJ m^{-2}). The nanostructuring and hydrogenating of a surface layer additionally reduce this shear stability.

The use of scanning tunneling microscopy permitted us [18] to reveal the mechanism of the extrusion of the material in a channelled nonlinear wave. It is seen from Fig. 4 that the wave extrusion of the material occurs as a result of the mutual displacements of individual lamellae, with each lamella being extruded via mutual displacements of even finer transverse lamellae. The binormal to each lamella is perpendicular to the sample's plane and, consequently, to the direction of the counter field ∇f from the side of the crystalline substrate. These data indicate a hierarchically organized structure of the nonlinear wave of the extrudible material. Correspondingly, a linear dependence should exist between the quantities δ and λ at each scale level. This is indeed confirmed experimentally.

Figure 3d displays the $\delta = f(\lambda)$ dependence calculated from the data of Ref. [14] for a ferritic–martensitic steel. This dependence corresponds to a straight line $\delta = k\lambda$ with a coefficient $k = 0.75$. The three scales of nonlinear waves shown in Fig. 4 are also described by a linear dependence $\delta = k_1\lambda$ (Fig. 4b) if the length of the lamella is assumed to be $1/2\lambda$, and its thickness to be δ. The coefficient $k_1 = 0.17$ is a factor of 4.4 less than the coefficient k for steel. This means that in titanium with its low shear stability a mesoband of a given power at a distance equal to its wavelength λ is capable of traveling a distance that is a factor of 4.4 greater than an analogous mesoband at a distance equal to its wavelength in high-strength steel. This regularity is also confirmed by the characteristics of nonlinear waves in nanostructured surface layers of other materials.

A good agreement between the predictions of the gauge theory of nonlinear waves of channelled structural transformations in planar subsystems and the experimental data indicates the validity of the conception of the authors of this paper focused on the necessity of representation of surface layers and internal interfaces as the leading functional subsystem in a deformable solid. The theoretical and experimental investigations of nonlinear waves of channelled plastic flow in planar subsystems with allowance for the well-developed theory of strain-induced defects in crystals opens the way for constructing a general theory of a deformable solid as a nonlinear hierarchically organized system [4].

5. Nonlinear wave processes of fracture

In general, the fracture of a solid constitutes a dissipative process. A crack represents a rotation deformation mode on a macroscale level. According to the law of conservation of angular momentum, this mode should be equal to the sum of rotation modes at lower scale levels. In a continuum medium, this is a dissipative process.

However, if we create conditions for a channelled propagation of a crack and maximally localize the dissipation effects, the crack will propagate via a nonlinear wave mechanism. This follows from the nonequilibrium thermodynamics of its propagation. The opening of a crack is caused by the structural phase decomposition of the material ahead of its tip, and this is a threshold process. The propagation of a crack is related to the relaxation of the stress concentrator in its tip. The growth of a crack should periodically cease for the restoration of the stress concentrator and the establishment of the state of structural phase decomposition in a new zone of the material. This is a typical nonlinear wave process which can be described by equation (6) if we neglect the term $P_v^{\beta} C_{\alpha\beta}^{\mu\nu}/E$ in it. An increase of the term $\partial \ln u_\alpha(x,t)/\partial x_\mu$ related to normal stresses will be periodically compensated for by quasielastic forces that are represented by the second term, $(\partial \ln u_\beta/\partial x_\nu)\, C_{\alpha\beta}^{\mu\nu}/E$. This will cause a nonlinear wave character of the propagation of the crack with periodic stops. Naturally, the rate of change of the right-hand part of Eqn (6) should be small for revealing such wave processes, i.e., the nonlinear fracture waves should be slow.

Such wave processes of a channelled fracture were described in paper [17] for the case of the propagation of fatigue cracks in two-layer composites. At first, zigzag mesobands of localized plastic deformation developed at the interface of unlike media in the course of their cyclic alternate bending. Then, a channelled fatigue crack of shears–rotations propagated as a nonlinear wave process in one of the mesobands.

In recent work [24], the channeling of fractures and the minimization of dissipation processes were realized in the case of tension of planar samples of submicrocrystalline titanium with a chevron notch (Fig. 6a). Under the conditions of uniaxial tension, an opening mode crack was nucleated in the tip C of a thin planar layer in the form of a chevron notch, which propagated in a channeling mode along the longitudinal section of the sample. The high degree of departure from thermodynamic equilibrium of the submicrocrystalline state caused rapid structural phase decomposition of the material in the region ahead of the crack tip. Further in this region, a transverse fracture wave propagated, which shifted

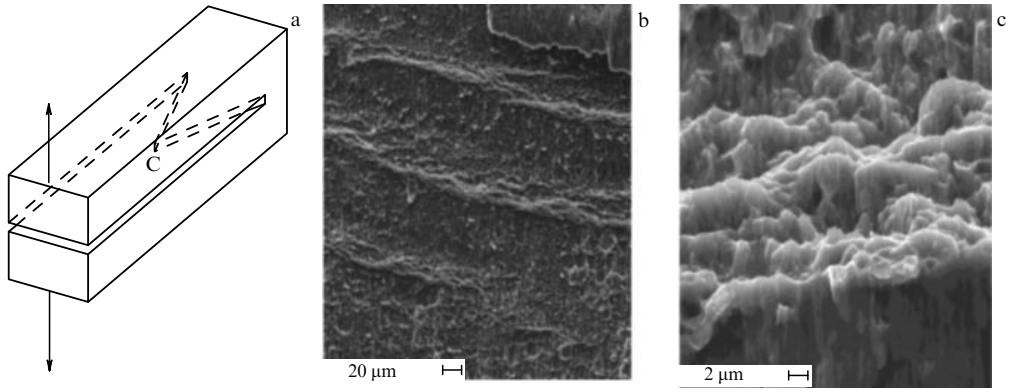

Figure 6. Nonlinear waves on the fracture surface after tensile test of a sample with a chevron notch [24]: (a) shape of the sample; (b) periodic white transverse bands of the material which underwent structural phase decomposition, and (c) porous nanostructure of a transverse band of the material. The micrographs were obtained using scanning electron microscopy.

the decomposition products of the crystalline material toward the periphery of this region (Fig. 6b). The porous nanostructure of the material that underwent a structural phase decomposition and was rejected by the fracture wave to the periphery of the transverse band is demonstrated in Fig. 6c. This material exhibits secondary-electron emission and can thus easily be detected. These results are of important value for the explanation of the fracture mechanism in solids.

Such nonlinear fracture wave processes are characteristic of many nanostructured objects (multilayer nanostructured coatings, thin-film structures in microelectronics, nanostructured surface layers of a functional designation in materials science, etc.). These wave processes can be controlled on the basis of the theory developed in paper [10].

6. Conclusions

It is suggested that a deformable solid be treated as a nonlinear hierarchically organized system consisting of two self-consistent subsystems. The deformation of a three-dimensional translationally invariant crystalline subsystem is described on the basis of the theory of strain-induced defects. In this case, local structural transformations in the cores of the strain-induced defects and an increase in the magnitude of departure from thermodynamic equilibrium of the deformable crystal should be taken into account. The surface layers and all internal interfaces should be considered as an independent planar nonlinear subsystem with a disrupted translational invariance rather than as planar defects in a three-dimensional crystal. The primary plastic shears in a loaded solid are related to the nonlinear waves of channelled structural transformations in a planar subsystem rather than to dislocations. The propagation of nonlinear channelled waves is accompanied by a periodic generation of strain-induced defects in the zones of strong curvature, whose emission into the crystalline subsystem provides a plastic change of its shape.

A theoretical and experimental substantiation of the conception developed is given. It is shown that the theory of nonlinear waves of channelled plastic deformation developed in paper [10] satisfactorily describes the regularities of the development of nonlinear wave processes which determine the law of self-consistency of plastic flow in multiscale hierarchically organized systems. The violation of such self-consistency leads to the fracture of a loaded solid. The nonequilibrium thermodynamics of fracture is related to the structural phase decomposition of the condensed state of a solid in regions where the Gibbs thermodynamic potential proves to be positive. The channelled propagation of cracks in multiscale systems is also developed as a nonlinear wave process.

Acknowledgments. This work was supported in part by the Siberian Branch of the Russian Academy of Sciences (project Nos III.20.1.1 and 72); by the Presidium of the Russian Academy of Sciences (project Nos 2.2 and 25.3); by the Russian Foundation for Basic Research (project No. 10.01.13300-RT_OMI), and by the President of the Russian Federation (project No. NSh-6116.2012.1).

References

1. Panin V E, Likhachev V A, Grinyaev Yu V *Strukturnye Urovni Deformatsii Tverdykh Tel* (Structural Levels of Deformation of Solids) (Novosibirsk: Nauka, 1985)
2. Meyers M A, Chawla K K *Mechanical Behavior of Materials* (Upper Saddle River, NJ: Prentice Hall, 1999)
3. Panin V E, Egorushkin V E, Panin A V *Fiz. Mezomekh.* **13** (5) 7 (2010) [*Phys. Mesomech.* **13** 215 (2010)]
4. Panin V E, Egorushkin V E *Fiz. Mezomekh.* **14** (3) 7 (2011) [*Phys. Mesomech.* **14** 207 (2011)]
5. Panin V E, Egorushkin V E, Panin A V *Fiz. Mezomekh.* **15** (1) 7 (2012) [*Phys. Mesomech.* **15** (2) (2012)]
6. Leontovich M A *Zh. Eksp. Teor. Fiz.* **8** 844 (1938)
7. Panin V E, Egorushkin V E, Panin A V, Moiseenko D D *Zh. Tekh. Fiz.* **77** (8) 62 (2007) [*Tech. Phys.* **52** 1024 (2007)]
8. Panin V E et al. *Izv. Vyssh. Uchebn. Zaved. Fiz.* **30** (1) 34 (1987) [*Sov. Phys. J.* **30** 24 (1987)]
9. Egorushkin V E *Izv. Vyssh. Uchebn. Zaved. Fiz.* **33** (2) 51 (1990) [*Sov. Phys. J.* **33** 135 (1990)]
10. Egorushkin V E *Izv. Vyssh. Uchebn. Zaved. Fiz.* **35** (4) 19 (1992) [*Sov. Phys. J.* **35** 316 (1992)]
11. Panin V E, Panin A V *Fiz. Mezomekh.* **8** (5) 7 (2005) [*Phys. Mesomech.* **8** (5 – 6) 7 (2005)]
12. Panin A V *Fiz. Mezomekh.* **8** (3) 5 (2005) [*Phys. Mesomech.* **8** (3 – 4) 5 (2005)]
13. Panin V E et al., in *Poverkhnostnye Sloi i Vnutrennie Granitsy Razdela v Geterogennykh Materialakh* (Surface Layers and Internal Interfaces in Heterogeneous Materials) (Exec. Ed. V E Panin) (Novosibirsk: Izd. SO RAN, 2006)
14. Panin A V et al. *J. Nucl. Mater.* **386 – 388** 466 (2009)
15. Deryugin E E et al. *Fiz. Mezomekh.* **4** (3) 35 (2001) [*Phys. Mesomech.* **4** (3) 35 (2001)]

16. Elsukova T F, Panin V E *Fiz. Met. Metalloved.* **97** (1) 121 (2004) [*Phys. Met. Metallogr.* **97** 111 (2004)]
17. Panin V E, Elsukova T F, Popkova Yu F *Dokl. Ross. Akad. Nauk* **443** 40 (2012) [*Dokl. Phys.* **57** 100 (2012)]
18. Panin V E *Fiz. Met. Metalloved.* **98** (1) 109 (2004) [*Phys. Met. Metallogr.* **98** 98 (2004)]
19. Zuev L B, Barannikova S A *Natural Science* **2** 476 (2010)
20. Kadić A, Edelen D G B *A Gauge Theory of Dislocations and Disclinations* (Berlin: Springer-Verlag, 1983) [Translated into Russian (Moscow: Mir, 1987)]
21. Lagoudas D C, Edelen D G B *Int. J. Eng. Sci.* **27** 411 (1989)
22. Cünther H *Ann. Physik* **495** 291 (1983)
23. McConnell A J *Application of Tensor Analysis* (New York: Dover Publ., 1957) [Translated into Russian (Moscow: Fizmatlit, 1963)]
24. Panin V E et al. *Fiz. Mezomekh.* **15** (6) 5 (2012) [*Phys. Mesomech.* **16** (2) 81 (2013)]